

Travelling wave solutions of the perturbed mKdV equation that represent traffic congestion

Laura Hattam *

Abstract

A well-known optimal velocity (OV) model describes vehicle motion along a single lane road, which reduces to a perturbed modified Korteweg-de Vries (mKdV) equation within the unstable regime. Steady travelling wave solutions to this equation are then derived with a multi-scale perturbation technique. The first order solution in the hierarchy is written in terms of slow and fast variables. At the following order, a system of differential equations are highlighted that govern the slowly evolving properties of the leading solution. Then, it is shown that the critical points of this system signify travelling waves without slow variation. As a result, a family of steady waves with constant amplitude and period are identified. When periodic boundary conditions are satisfied, these solutions' parameters are associated with the driver's sensitivity, \hat{a} , which appears in the OV model. For some given \hat{a} , solutions of both an upward and downward form exist, with the downward type corresponding to traffic congestion. Numerical simulations are used to validate the asymptotic analysis and also to examine the long-time behaviour of our solutions.

1 Introduction

To minimise congestion it is necessary to understand traffic behaviour, which has led to many traffic related studies with varied perspectives. Nagatani [2002] has given an overview of the different methods that analyse vehicle motion. One option is the application of a macroscopic model to characterise vehicle headway. The following optimal velocity (OV) model is an example of this approach,

$$\frac{d^2 \Delta x_j}{dt^2} = \hat{a} \left(V(\Delta x_{j+1}(t)) - V(\Delta x_j(t)) - \frac{d\Delta x_j}{dt} \right), \quad (1)$$

where $x_j(t)$ is the position of car j at time t , $\Delta x_j = x_{j+1} - x_j$ is car j 's headway, V is the car's optimal velocity, $j = 0, 1, 2, \dots, N$ for N cars on the road and \hat{a} is the driver's sensitivity. This equation was derived by Bando et al. [1995] to describe vehicle behaviour on a single lane road. As well, they proposed the optimal velocity function,

$$V(\Delta x_j(t)) = \frac{v_{max}}{2} (\tanh(\Delta x_j - h_c) + \tanh(h_c)), \quad (2)$$

where h_c is the safety distance and v_{max} is the maximal velocity.

Applying linear stability analysis to (1), a neutral stability line with a critical point is obtained. This line signifies the boundary between two stability regions referred to as metastable and unstable. See Ge et al. [2005] for further detail.

Muramatsu and Nagatani [1999] reduced (1) to a perturbed Korteweg-de Vries (KdV) equation within the metastable zone using nonlinear theory. This was the KdV equation with higher order correction terms. They numerically identified traffic solitons propagating over open boundaries, which eventually

*University of Reading

dissolved. This behaviour is expected within this stability regime since all solutions should tend to the uniform headway. Hattam [2016] studied this problem with periodic boundaries, where cnoidal waves were shown to exist that represented traffic congestion. These solutions were derived with multi-scale analysis and then validated with numerical simulations. Again, these density waves disappeared after some time.

Whereas, solutions corresponding to the unstable region were identified by Komatsu and Sasa [1995]. Beginning with (1) close to the critical point along the neutral stability line, they derived a perturbed modified KdV (mKdV) equation. The leading order solution to this equation was written in terms of Jacobi elliptic functions that were dependent on the elliptic modulation term $m \in [0, 1]$. When $m = 1$, this solution became the kink soliton, which exhibits the start/stop motion representative of a traffic jam.

Komatsu and Sasa [1995] applied perturbation analysis to seek steady travelling wave solutions of the mKdV traffic model. They established that this solution type only existed when the wave modulus m remained constant and consequently, this wave amplitude and period were fixed. A condition for m as some constant was found in terms of integral constraints that then determined the relationship between m and the wave speed. They referred to the travelling wave solutions with $m = 1$ as deformed kink solitons. Otherwise, for constant $m \neq 1$, they were called deformed periodic solitons.

Here, a multi-scale perturbation technique is applied to the perturbed mKdV equation to also identify steady travelling wave solutions. This approach is an adaptation of the method outlined by Hattam and Clarke [2015] for the steady forced KdV-Burgers equation. Solutions of a similar form to the deformed periodic solitons found by Komatsu and Sasa [1995] are highlighted, which satisfy periodic boundaries. Komatsu and Sasa [1995] proposed that this solution type was always unstable and only deformed kink solitons were observed numerically. The stability of our periodic waves is investigated here.

Such studies as Zhu and Dai [2008] and Zheng et al. [2012] have numerically examined OV traffic models within the unstable zone, where periodic boundary conditions were imposed. The long-time behaviour was analysed, which revealed solutions that were indicative of mKdV dynamics as kink-like waves appeared. Moreover, Li et al. [2015] performed numerical simulations over large time intervals of an OV model that described a two-lane system with periodic boundaries. As well, this model was transformed into a perturbed mKdV equation near to the critical point. The numerical results corresponding to this region uncovered steady periodic travelling wave solutions with constant amplitude, mean height and period. Hence, these numerical findings suggest stable periodic solutions to the OV traffic system do propagate within this unstable regime.

The focus of this paper is the derivation of steady travelling wave solutions to (1) and then the analysis of their long-time dynamics. In Section 2, (1) is reduced to a perturbed mKdV equation and then steady travelling wave solutions are determined using a multi-scale perturbation method in Section 3. The leading order solution is obtained in terms of Jacobi elliptic functions that depend upon slow and fast variables. At the next order, a dynamical system governing the slow variation of the leading order solution is identified. Then, in Section 4, the fixed points of this system are shown to represent a family of steady travelling waves that do not slowly vary. This set of solutions have fixed amplitude, mean height and period. Also, the relations between the solution parameters, the wave speed and the driver's sensitivity are established due to implementing periodic boundary conditions. Lastly, in Section 5, the highlighted periodic asymptotic solutions are compared with numerical results.

2 Traffic Flow Model

We now outline how the OV model (1) was transformed by Ge et al. [2005] into a perturbed mKdV equation. This then becomes the steady perturbed Gardner equation when we seek steady travelling wave solutions.

Firstly, Ge et al. [2005] deduced for the system (1), the linear stability criteria

$$\hat{a} \geq \hat{a}_s = 2V'(h), \quad (3)$$

where h is the uniform headway. When this is met, the steady state of $\Delta x_j(t) = h$ is stable. The curve defined by $\hat{a} = \hat{a}_s$ is the ‘neutral stability line’, which indicates the onset of instability. This curve’s critical point occurs at $h = h_c$ and $\hat{a} = \hat{a}_c = 2V'(h_c)$. The region neighbouring this point is where the perturbed mKdV equation applies.

Next, Ge et al. [2005] used the change of variables

$$\bar{x} = \epsilon(j + V'(h_c)t), \quad \bar{t} = \epsilon^3 g_1 t, \quad \epsilon^2 = (\hat{a}_c/\hat{a}) - 1, \quad 0 < \epsilon \ll 1, \quad (4)$$

and let

$$\Delta x_j(t) = h_c + \epsilon \sqrt{\frac{g_1}{g_2}} R, \quad (5)$$

where they introduced

$$g_1 = V'(h_c)/6, \quad g_2 = -V'''(h_c)/6, \quad g_3 = V'(h_c)/2, \quad g_4 = V'(h_c)/8, \quad g_5 = V'''(h_c)/12. \quad (6)$$

As a result, (1) reduced to

$$R_{\bar{t}} - R_{\bar{x}\bar{x}\bar{x}} + 3R^2 R_{\bar{x}} + \epsilon \left(\frac{g_3}{\sqrt{g_1}} R_{\bar{x}\bar{x}} + \frac{g_4}{\sqrt{g_1}} R_{\bar{x}\bar{x}\bar{x}\bar{x}} + \sqrt{g_1} \frac{g_5}{g_2} \partial_{\bar{x}\bar{x}}(R^3) \right) = 0, \quad (7)$$

where $O(\epsilon^2)$ terms are ignored, which is a perturbed mKdV equation. Since $\epsilon > 0$ is small and therefore $\hat{a} < \hat{a}_c$, the stability criteria (3) does not hold and the solutions to (7) are unstable. Thus, this is the unstable regime.

Here, steady travelling wave solutions of (7) are sought. To identify this solution type, we set

$$\tilde{x} = \bar{x} - \omega \bar{t},$$

where ω is the constant wave speed. As well, if $\sqrt{\omega}u = R + \sqrt{\frac{\omega}{3}}$, (7) becomes

$$\lambda u_{\tilde{x}\tilde{x}\tilde{x}} - \gamma u^2 u_{\tilde{x}} + \nu u u_{\tilde{x}} + \epsilon G(u, \tilde{x}) = 0, \quad (8)$$

where

$$\lambda = 1, \quad \gamma = 3\omega, \quad \nu = 2\sqrt{3}\omega, \quad (9)$$

and

$$G(u, \tilde{x}) = - \left(\frac{g_3}{\sqrt{g_1}} u_{\tilde{x}\tilde{x}} + \frac{g_4}{\sqrt{g_1}} u_{\tilde{x}\tilde{x}\tilde{x}\tilde{x}} + \omega \sqrt{g_1} \frac{g_5}{g_2} \partial_{\tilde{x}\tilde{x}} \left(\left(u - \frac{1}{\sqrt{3}} \right)^3 \right) \right). \quad (10)$$

The system (8) is the steady perturbed Gardner equation. The parameters λ, γ, ν have been introduced so that initially the analysis is generalised.

3 Perturbation Analysis

The modulation theory detailed by Hattam and Clarke [2015] for the steady perturbed KdV equation is now applied to (8). However, since an additional cubic nonlinear term must be considered, the modulation theory for the Gardner equation is also used, which was outlined by Kamchatnov et al. [2012]. As a result of this perturbation analysis, a leading order solution to (8) is highlighted that varies with slow and fast variables. Then at the next order, equations are found that describe the slow evolution of this solution.

To begin, let

$$X = \epsilon \tilde{x}, \quad \theta_X = \frac{1}{\epsilon} k(X), \quad (11)$$

and

$$u(\tilde{x}) = u_0(\theta, X) + \epsilon u_1(\theta, X) + \epsilon^2 u_2(\theta, X) + \dots, \quad (12)$$

where X and θ are ‘slow’ and ‘fast’ variables respectively.

Consequently, (8) takes the form at first and second order

$$O(1) : \lambda k^2 u_{0,\theta\theta\theta} - \gamma u_0^2 u_{0,\theta} + \nu u_0 u_{0,\theta} = 0, \quad (13a)$$

$$O(\epsilon) : \lambda k^3 u_{1,\theta\theta\theta} - \gamma k (u_0^2 u_1)_\theta + \nu k (u_0 u_1)_\theta + g = 0, \quad (13b)$$

where

$$g(\theta, X) = G(\theta, X) + 3\lambda k^2 u_{0,\theta\theta X} - \gamma u_0^2 u_{0,X} + \nu u_0 u_{0,X} + 3\lambda k k_X u_{0,\theta\theta}. \quad (14)$$

The integration of (13a) twice gives

$$\frac{6\lambda k^2}{\gamma} u_{0,\theta}^2 = u_0^4 - \frac{2\nu}{\gamma} u_0^3 + \frac{12}{\gamma} \hat{C} u_0 + \frac{12}{\gamma} \hat{D}, \quad (15)$$

where \hat{C} and \hat{D} are integration constants. Next, let

$$Q(u_0) = u_0^4 - \frac{2\nu}{\gamma} u_0^3 + \frac{12}{\gamma} \hat{C} u_0 + \frac{12}{\gamma} \hat{D}, \quad (16)$$

where Q is a polynomial of order 4. Suppose that $a \leq b \leq c \leq d$ are the roots of this polynomial, then

$$u_0^4 - \frac{2\nu}{\gamma} u_0^3 + \frac{12}{\gamma} \hat{C} u_0 + \frac{12}{\gamma} \hat{D} = Q(u_0) = (u_0 - a)(u_0 - b)(u_0 - c)(u_0 - d). \quad (17)$$

By expanding the righthand side of (17) and equating like terms, we find

$$\frac{2\nu}{\gamma} = a + b + c + d, \quad (18a)$$

$$\frac{12\hat{C}}{\gamma} = -(acd + abd + abc + bcd), \quad (18b)$$

$$\frac{12\hat{D}}{\gamma} = abcd, \quad (18c)$$

$$0 = bc + ac + cd + ab + bd + ad. \quad (18d)$$

So the equation parameters are dependent upon the roots a, b, c, d . As well, since $Q(u_0 = a, b, c, d) = 0$, then

$$a\hat{C} + \hat{D} = \frac{\nu a^3}{6} - \frac{\gamma a^4}{12}, \quad (19a)$$

$$b\hat{C} + \hat{D} = \frac{\nu b^3}{6} - \frac{\gamma b^4}{12}, \quad (19b)$$

$$c\hat{C} + \hat{D} = \frac{\nu c^3}{6} - \frac{\gamma c^4}{12}, \quad (19c)$$

$$d\hat{C} + \hat{D} = \frac{\nu d^3}{6} - \frac{\gamma d^4}{12}. \quad (19d)$$

The solution to (13a) can also be written in terms of these roots, such that

$$u_0(\theta, X) = \frac{ce + d \operatorname{sn}^2(\beta(\theta - \theta_0); m)}{e + \operatorname{sn}^2(\beta(\theta - \theta_0); m)}, \quad (20)$$

where

$$\frac{24\lambda\beta^2 k^2}{\gamma} = (a - c)(b - d), \quad (21a)$$

$$e = -\left(\frac{b - d}{b - c}\right), \quad (21b)$$

$$m^2 = \frac{(a - d)(b - c)}{(a - c)(b - d)}, \quad (21c)$$

$$\beta = K(m)/P. \quad (21d)$$

The period of (20) is $2P$, where P is some fixed constant. The function sn is the Jacobi elliptic function, $m \in [0, 1]$ is its elliptic modulus and the function $K(m)$ is the complete elliptic integral of the first kind. The parameters a, b, c, d, m, θ_0 are all dependent on the slow variable X .

To ensure the next order solution, u_1 , has the period $2P$, the periodicity conditions

$$\frac{1}{2P} \int_{\theta_1}^{\theta_2} g(\theta, X) d\theta = 0, \quad (22a)$$

$$\frac{1}{2P} \int_{\theta_1}^{\theta_2} g(\theta, X) u_0 d\theta = 0, \quad (22b)$$

are imposed, where $\theta_1 = -P + \theta_0$ and $\theta_2 = P + \theta_0$. Note that u_0 and its derivatives with respect to θ are assumed to be periodic over the domain $\theta \in [\theta_1, \theta_2]$. The integral (22b) written in full is

$$\frac{1}{2P} \int_{\theta_1}^{\theta_2} G u_0 d\theta + \frac{1}{2P} I_b = 0, \quad (23)$$

where

$$\begin{aligned} I_b &= \int_{\theta_1}^{\theta_2} (3\lambda(k^2 u_{0,\theta\theta X} + k k_X u_{0,\theta\theta}) - \gamma u_0^2 u_{0,X} + \nu u_0 u_{0,X}) u_0 d\theta \\ &= \partial_X \int_{\theta_1}^{\theta_2} \left(-\frac{3\lambda k^2}{2} u_{0,\theta}^2 - \frac{\gamma}{4} u_0^4 + \frac{\nu}{3} u_0^3 \right) d\theta. \end{aligned} \quad (24)$$

Next, by manipulating (15), it can be shown

$$\frac{3\gamma}{2P} \int_{\theta_1}^{\theta_2} u_0^4 d\theta = \frac{5\nu}{2P} \int_{\theta_1}^{\theta_2} u_0^3 d\theta - \frac{18\hat{C}}{2P} \int_{\theta_1}^{\theta_2} u_0 d\theta - 12\hat{D}, \quad (25a)$$

$$\frac{18\lambda k^2}{2P} \int_{\theta_1}^{\theta_2} u_{0,\theta}^2 d\theta = -\frac{\nu}{2P} \int_{\theta_1}^{\theta_2} u_0^3 d\theta + \frac{18}{2P} \hat{C} \int_{\theta_1}^{\theta_2} u_0 d\theta + 24\hat{D}. \quad (25b)$$

Hence,

$$-\frac{18\lambda k^2}{2P} \int_{\theta_1}^{\theta_2} u_{0,\theta}^2 d\theta + \frac{1}{2P} \int_{\theta_1}^{\theta_2} (-3\gamma u_0^4 + 4\nu u_0^3) d\theta = -12\hat{D},$$

and therefore, (24) takes the form

$$\frac{1}{2P} I_b = -\hat{D}_X.$$

As well, the integral (22a) can be written

$$\frac{1}{2P} \int_{\theta_1}^{\theta_2} G d\theta + \frac{1}{2P} I_a = 0, \quad (26)$$

where

$$\begin{aligned} I_a &= \int_{\theta_1}^{\theta_2} \left(3\lambda(k^2 u_{0,\theta\theta X} + k k_X u_{0,\theta\theta}) - \frac{\gamma}{3} (u_0^3)_X + \frac{\nu}{2} (u_0^2)_X \right) d\theta \\ &= \partial_X \int_{\theta_1}^{\theta_2} \left(-\frac{\gamma}{3} u_0^3 + \frac{\nu}{2} u_0^2 \right) d\theta, \\ &= 2\hat{C}_X, \end{aligned}$$

using (15).

Thus, the integral conditions (22) reduce to

$$\hat{C}_X = -\frac{1}{2P} \int_{\theta_1}^{\theta_2} G(\theta, X) d\theta, \quad (27a)$$

$$\hat{D}_X = \frac{1}{2P} \int_{\theta_1}^{\theta_2} G(\theta, X) u_0 d\theta. \quad (27b)$$

This system determines the slow variation of the leading order solution (20) for some given function $G(\theta, X)$.

3.1 Application to the traffic flow model

So to locate steady travelling wave solutions of the traffic model (1), G is now defined by (10). Firstly,

$$\int_{\theta_1}^{\theta_2} G(\theta, X) d\theta = -\omega \sqrt{g_1} \frac{g_5}{g_2} k^2 \left[3 \left(u_0 - \frac{1}{\sqrt{3}} \right)^2 u_{0,\theta} \right]_{\theta_1}^{\theta_2} = 0,$$

where $O(\epsilon)$ terms are ignored. Therefore, if κ_1 is some constant, from (27a),

$$\hat{C} = \kappa_1. \quad (28)$$

Next let us set $\hat{D}_X = \tilde{I}$, so that

$$\tilde{I} = \frac{1}{2P} \int_{\theta_1}^{\theta_2} G(\theta, X) u_0 d\theta.$$

Given (10), this integral becomes

$$\begin{aligned} \tilde{I} &= -\frac{1}{2P} \int_{\theta_1}^{\theta_2} u_0 \left(\frac{g_3}{\sqrt{g_1}} k^2 u_{0,\theta\theta} + \frac{g_4}{\sqrt{g_1}} k^4 u_{0,\theta\theta\theta\theta} + \omega \sqrt{g_1} \frac{g_5}{g_2} k^2 \partial_{\theta\theta} \left(\left(u_0 - \frac{1}{\sqrt{3}} \right)^3 \right) \right) d\theta \\ &= -\frac{1}{2P} \int_{\theta_1}^{\theta_2} \left(\frac{g_3}{\sqrt{g_1}} k^2 u_0 u_{0,\theta\theta} + \frac{g_4}{\sqrt{g_1}} k^4 u_0 u_{0,\theta\theta\theta\theta} - \omega \sqrt{g_1} \frac{g_5}{g_2} k^2 u_{0,\theta} \partial_{\theta} \left(\left(u_0 - \frac{1}{\sqrt{3}} \right)^3 \right) \right) d\theta \\ &= -\frac{1}{2P} \int_{\theta_1}^{\theta_2} \left(-\frac{g_3}{\sqrt{g_1}} k^2 u_0^2 + \frac{g_4}{\sqrt{g_1}} k^4 u_0 u_{0,\theta\theta\theta\theta} - 3\omega \sqrt{g_1} \frac{g_5}{g_2} k^2 u_{0,\theta}^2 \left(u_0^2 - \frac{2}{\sqrt{3}} u_0 + \frac{1}{3} \right) \right) d\theta. \end{aligned} \quad (29)$$

Hence, to write \tilde{I} in full we must solve the integrals

$$\tilde{I}_1 = \frac{1}{2P} \int_{\theta_1}^{\theta_2} u_0^2 d\theta, \quad \tilde{I}_2 = \frac{1}{2P} \int_{\theta_1}^{\theta_2} u_0 u_{0,\theta\theta\theta\theta} d\theta, \quad \tilde{I}_3 = \frac{1}{2P} \int_{\theta_1}^{\theta_2} u_0^2 u_{0,\theta}^2 d\theta, \quad \tilde{I}_4 = \frac{1}{2P} \int_{\theta_1}^{\theta_2} u_0 u_{0,\theta\theta\theta\theta} d\theta.$$

As a result of manipulating (15), the integrals \tilde{I}_1 , \tilde{I}_2 and \tilde{I}_3 are determined. Omitting the details here, we arrive at

$$\tilde{I}_1 = \frac{1}{\lambda k^2} \left(-\frac{\nu^2}{12\gamma} \alpha_2 + \left(\alpha_1 + \frac{\nu}{6\gamma} \right) \hat{C} + \frac{4}{3} \hat{D} \right), \quad (30a)$$

$$\tilde{I}_2 = \frac{\gamma}{6\lambda k^2} \left(\alpha_2 \left(\frac{9\hat{C}}{2\gamma} - \frac{5\nu^3}{8\gamma^3} \right) + \alpha_1 \left(\frac{6\hat{D}}{\gamma} + \frac{3\nu\hat{C}}{2\gamma^2} \right) + \frac{5\nu^2\hat{C}}{4\gamma^3} + \frac{\nu\hat{D}}{\gamma^2} \right), \quad (30b)$$

$$\tilde{I}_3 = \frac{\gamma}{6\lambda k^2} \left(\alpha_2 \left(\frac{69\hat{C}\nu}{10\gamma^2} - \frac{7\nu^4}{8\gamma^4} + \frac{24\hat{D}}{5\gamma} \right) + \alpha_1 \left(\frac{6\nu\hat{D}}{5\gamma^2} + \frac{21\nu^2\hat{C}}{10\gamma^3} \right) + \frac{35\nu^3\hat{C}}{20\gamma^4} + \frac{7\nu^2\hat{D}}{5\gamma^3} - \frac{54\hat{C}^2}{5\gamma^2} \right), \quad (30c)$$

where

$$\alpha_1(m, c, d, e) = \frac{1}{2P} \int_{\theta_1}^{\theta_2} u_0 d\theta, \quad \alpha_2(m, c, d, e) = \frac{1}{2P} \int_{\theta_1}^{\theta_2} u_0^2 d\theta. \quad (31)$$

Refer to the Appendix for the evaluation of these integrals.

Next, the integral \tilde{I}_4 can be written, from (13a),

$$\begin{aligned} \tilde{I}_4 &= \frac{1}{2P} \int_{\theta_1}^{\theta_2} u_0 u_{0,\theta\theta\theta\theta} d\theta = -\frac{1}{2P} \int_{\theta_1}^{\theta_2} u_{0,\theta} u_{0,\theta\theta\theta} d\theta \\ &= -\frac{1}{2P} \int_{\theta_1}^{\theta_2} u_{0,\theta} \left(\frac{\gamma}{\lambda k^2} u_0^2 u_{0,\theta} - \frac{\nu}{\lambda k^2} u_0 u_{0,\theta} \right) d\theta \\ &= -\frac{\gamma}{\lambda k^2} \tilde{I}_3 + \frac{\nu}{\lambda k^2} \tilde{I}_2. \end{aligned}$$

Thus, (29) reduces to

$$\tilde{I} = k^2 \tilde{I}_1 \left(\frac{g_3}{\sqrt{g_1}} + \frac{\sqrt{g_1} g_5 \omega}{g_2} \right) + k^2 \tilde{I}_2 \left(-\frac{\nu g_4}{\lambda \sqrt{g_1}} - \frac{2\sqrt{3}\omega \sqrt{g_1} g_5}{g_2} \right) + k^2 \tilde{I}_3 \left(\frac{g_4 \gamma}{\sqrt{g_1} \lambda} + \frac{3\omega \sqrt{g_1} g_5}{g_2} \right), \quad (32)$$

where \tilde{I}_1 , \tilde{I}_2 and \tilde{I}_3 are defined using (30).

4 Fixed Points

In Section 3, the leading order solution (20) to the traffic model (1) was obtained. Moreover, its slow variation was found to be governed by the system

$$\hat{C}_X = 0, \quad (33a)$$

$$\hat{D}_X = \tilde{I}, \quad (33b)$$

where \tilde{I} is given by (32). The critical points of this system occur when $\hat{D}_X = \tilde{I} = 0$, so that $\hat{D} = \kappa_2$, where κ_2 is some constant. We now want to highlight these fixed point solutions and show that they have constant wave amplitude, mean height and period.

Firstly, taking the derivative of (19a) with respect to X gives

$$\hat{D}_X = \frac{1}{6} (3a^2\nu - 2a^3\gamma - 6\kappa_1) a_X,$$

using $\hat{C} = \kappa_1$. Similarly, (19b)-(19d) take the form

$$\hat{D}_X = \frac{1}{6} (3b^2\nu - 2b^3\gamma - 6\kappa_1) b_X = \frac{1}{6} (3c^2\nu - 2c^3\gamma - 6\kappa_1) c_X = \frac{1}{6} (3d^2\nu - 2d^3\gamma - 6\kappa_1) d_X.$$

So, if $\hat{D}_X = 0$, then

$$a_X = b_X = c_X = d_X = 0, \quad (34)$$

(assuming $3a^2\nu - 2a^3\gamma - 6\kappa \neq 0$ etc.). As well, from (21c) it can be shown

$$\begin{aligned} \frac{2}{m} m_X = & a_X \left(\frac{1}{a-d} - \frac{1}{a-c} \right) + b_X \left(\frac{1}{b-c} - \frac{1}{b-d} \right) \\ & + c_X \left(\frac{1}{a-c} - \frac{1}{b-c} \right) + d_X \left(\frac{1}{b-d} - \frac{1}{a-d} \right). \end{aligned}$$

Therefore, when $\hat{D} = \kappa_2$ ($\tilde{I} = 0$), (34) is satisfied, and therefore

$$m_X = 0. \quad (35)$$

Hence, the fixed point solutions of the system (33) correspond to the leading order solution (20) with constant wave modulus m and constant solution parameters a, b, c, d, β . So then, these particular steady travelling waves do not have slowly varying properties, which means their amplitude, mean height and period remain fixed. Therefore, they are of a similar form to the deformed periodic solitons detailed by Komatsu and Sasa [1995].

It is necessary to determine when $\tilde{I} = 0$ to locate these fixed point solutions. Firstly, if the equation parameters λ and ν are defined using (9) and with $\hat{C} = \kappa_1$, $\hat{D} = \kappa_2$, (32) is written

$$\tilde{I} = k^2 \tilde{I}_1 \frac{g_3}{\sqrt{g_1}} + k^2 \omega \left(\tilde{I}_1 \frac{\sqrt{g_1} g_5}{g_2} + (3\tilde{I}_3 - 2\sqrt{3}\tilde{I}_2) \left(\frac{g_4}{\sqrt{g_1}} + \frac{\sqrt{g_1} g_5}{g_2} \right) \right), \quad (36)$$

where

$$\tilde{I}_1 = \frac{\gamma}{k^2} \left(\alpha_1 \frac{\kappa_1}{\gamma} - \frac{\alpha_2}{9} + \frac{\kappa_1}{3\sqrt{3}\gamma} + \frac{4\kappa_2}{3\gamma} \right), \quad (37a)$$

$$\tilde{I}_2 = \frac{\gamma}{6k^2} \left(\alpha_1 \left(\frac{3\kappa_1}{\sqrt{3}\gamma} + \frac{6\kappa_2}{\gamma} \right) + \alpha_2 \left(\frac{9\kappa_1}{2\gamma} - \frac{5}{\sqrt{3}} \right) + \frac{5\kappa_1}{\sqrt{3}\gamma} + \frac{2\kappa_2}{\sqrt{3}\gamma} \right), \quad (37b)$$

$$\tilde{I}_3 = \frac{\gamma}{6k^2} \left(\alpha_1 \left(\frac{14\kappa_1}{5\gamma} + \frac{12\kappa_2}{5\sqrt{3}\gamma} \right) + \alpha_2 \left(\frac{69\kappa_1}{5\sqrt{3}\gamma} + \frac{24\kappa_2}{5\gamma} - \frac{14}{9} \right) + \frac{14\kappa_1}{3\sqrt{3}\gamma} + \frac{28\kappa_2}{15\gamma} - \frac{54}{5} \left(\frac{\kappa_1}{\gamma} \right)^2 \right). \quad (37c)$$

Next, by setting $\tilde{I} = 0$, a definition for the constant wave speed is obtained as a function of κ_1/γ , κ_2/γ , $\alpha_1(m, c, d, e)$, $\alpha_2(m, c, d, e)$ and h_c , such that

$$\omega = -\frac{\rho_1}{\rho_2}, \quad (38)$$

where

$$\rho_1 = \frac{g_3}{\sqrt{g_1}} \tilde{I}_1,$$

and

$$\rho_2 = \tilde{I}_1 \frac{\sqrt{g_1 g_5}}{g_2} + (3\tilde{I}_3 - 2\sqrt{3}\tilde{I}_2) \left(\frac{g_4}{\sqrt{g_1}} + \frac{\sqrt{g_1 g_5}}{g_2} \right).$$

As an aside, if the minimum and maximum headway are set to h_{min} and h_{max} respectively, we want solutions with $h_{min} \leq h_c \leq h_{max}$ ($\Delta x_j = h_c + O(\epsilon)$), which suggests $R_{min} \leq 0 \leq R_{max}$ (refer to (5)). Consequently, given $u_0 \in [b, c]$, any solution must have $b \leq 1/\sqrt{3}$ and $c \geq 1/\sqrt{3}$. However, from (19b) and (19c), so that both criterion are satisfied, it is required

$$\frac{\kappa_2}{\gamma} = \frac{1}{36} - \frac{1}{\sqrt{3}} \frac{\kappa_1}{\gamma}, \quad (39)$$

where κ_1/γ and κ_2/γ are some constants. A definition for κ_2/γ as a function of κ_1/γ has now been found. Next, rewriting (16) in terms of κ_1/γ and κ_2/γ gives

$$Q(z) = z^4 - \frac{4}{\sqrt{3}} z^3 + 12 \frac{\kappa_1}{\gamma} z + 12 \frac{\kappa_2}{\gamma}. \quad (40)$$

Finding the four roots of this polynomial determines the solution parameters a, b, c, d , and then m using (21c), for some given κ_1/γ and where κ_2/γ is defined by (39). So, a, b, c, d , as well as the wave modulus m are identified as a function of κ_1/γ , which are depicted along the top panel of Figure 1. Given this relation between m, a, b, c, d and the parameter κ_1/γ , we can then obtain the wave speed (38) as a function of κ_1/γ (with h_c set to 4 throughout), which is displayed on the bottom left of Figure 1 (the properties α_1 and α_2 depend upon m, c, d and $e = -(b-d)/(b-c)$). It should be noted that the shift θ_0 is arbitrary since it has no influence on the other solution parameters. So we set $\theta_0 = 0$ for the remainder of the paper.

4.1 Periodic boundaries

The parameters of the leading order solution (20) have been defined in terms of the constant κ_1/γ (see Figure 1). By now using the variables j and t that appear in the traffic model (1) and applying periodic boundary conditions, the connection between this constant and the driver's sensitivity, \hat{a} , is also established.

To begin, (20) is written in terms of j and t ,

$$u_0(j, t) = c + (d - c) \frac{\text{sn}^2 \left(\beta \left(k \left(\epsilon(j + V'(h_c)t) - \omega g_1 \epsilon^3 t \right) - \theta_0 \right); m \right)}{e + \text{sn}^2 \left(\beta \left(k \left(\epsilon(j + V'(h_c)t) - \omega g_1 \epsilon^3 t \right) - \theta_0 \right); m \right)}, \quad (41)$$

where (4) was used. To ensure this solution satisfies periodic boundary conditions, it is necessary for

$$\frac{2P}{k\epsilon} n = N, \quad (42)$$

where n is some positive integer representing the number of oscillations over the domain $j \in [0, N]$. However, from (21a), it is known

$$\left(\frac{P}{k} \right)^2 = \frac{8K(m)^2}{\omega(a-c)(b-d)}. \quad (43)$$

Therefore, combining (42) and (43), as well as using $\epsilon^2 = (\hat{a}_c/\hat{a}) - 1$, we arrive at

$$\frac{\hat{a}_c}{\hat{a}} = \frac{32K(m)^2 n^2}{\omega(a-c)(b-d)N^2} + 1.$$

Rearranging this, a definition for the driver's sensitivity is found,

$$\hat{a} = \frac{a_c \omega (a-c)(b-d) N^2}{32K(m)^2 n^2 + \omega(a-c)(b-d) N^2}. \quad (44)$$

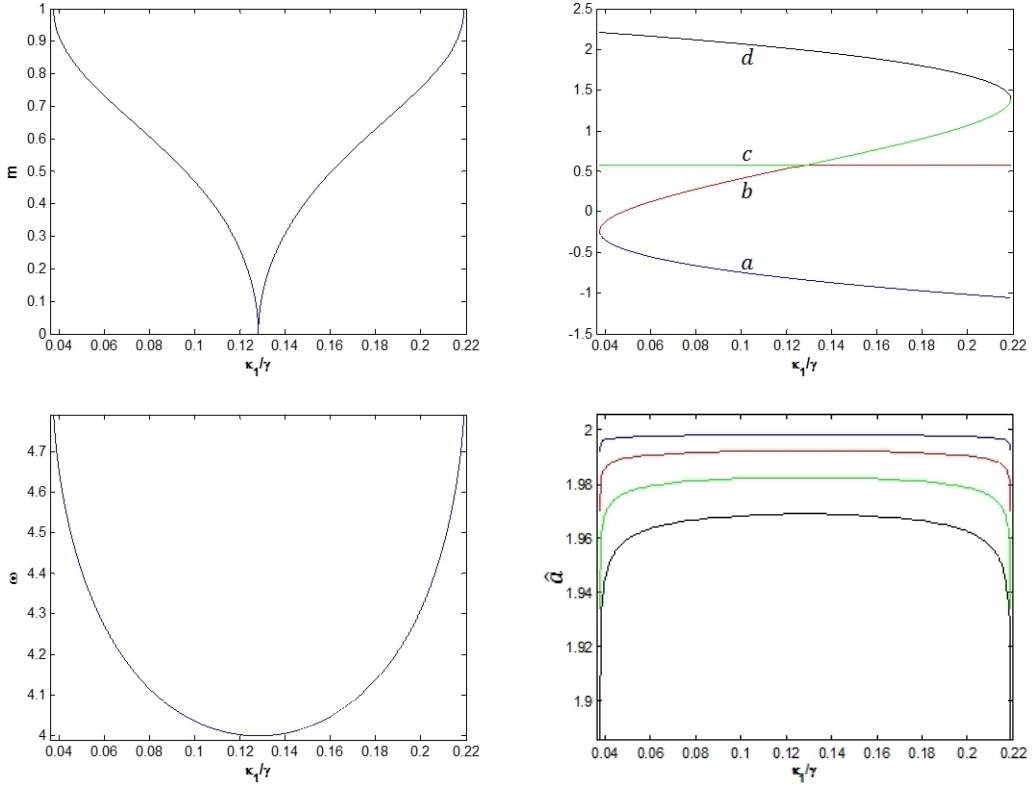


Figure 1: The parameter space for the periodic asymptotic solutions when $h_c = 4$. Top left: The plot of m , (21c), as a function of κ_1/γ . Top right: The plot of a (blue), b (red), c (green), d (black) as a function of κ_1/γ , which are the roots of (40). Bottom left: The plot of ω , (38), as a function of κ_1/γ . Bottom right: The plot of the driver's sensitivity \hat{a} , (44), as a function of κ_1/γ , where $N = 100$ and blue: $n = 1$, red: $n = 2$, green: $n = 3$, black: $n = 4$. Defining \hat{a} with (44) ensures periodic boundary conditions are satisfied.

For our fixed point solutions, the relationships between m, a, b, c, d, ω and κ_1/γ have been obtained (see Figure 1). Using these and (44), \hat{a} as a function of κ_1/γ is determined for some fixed n/N . This relation is plotted on the bottom right of Figure 1 for various n/N values. Note that when (44) holds, the solution will satisfy periodic boundary constraints. By relating \hat{a} to the asymptotic analysis then enables us to compare numerical solutions of the OV system (1) to our periodic solutions.

If \hat{a} and n/N are specified, from the curves shown in Figure 1, the wave modulus m (as well as a, b, c, d) and wave speed ω are identified. Hence, the solution parameters of (41) are defined by choosing \hat{a} and n/N . Moreover, Figure 1 reveals that for some fixed \hat{a} and n/N , there are two possible values for κ_1/γ , and therefore, two valid fixed point solutions. For the remainder of this paper, solutions with $\kappa_1/\gamma \lesssim 0.128$ ($\kappa_1/\gamma \gtrsim 0.128$) are referred to as the first (second) solution. The first solution represents traffic congestion since it is of a downward form with $u_0 \leq 1/\sqrt{3}$, which means the headway is less than or equal to the critical headway. Whereas, the second solution is of an upward form with $u_0 \geq 1/\sqrt{3}$. Note that when $m \rightarrow 0$, there is only one possible solution ($u_0 \rightarrow 1/\sqrt{3}$), where the headway tends to the constant state h_c .

Thus, a large family of spatially periodic steady travelling waves have been highlighted that do not slowly evolve, where their amplitude, mean height and period remain fixed. This solution type was discussed by Komatsu and Sasa [1995], where it was conjectured that they were always unstable. Note

however that a different parameter space was considered by Komatsu and Sasa [1995]. Next, the stability of our periodic solutions is examined.

5 Stability of periodic solutions

The asymptotic spatially periodic headway solutions are now fully defined, such that

$$\Delta x_j(t) = h_c + \epsilon \sqrt{\frac{\omega g_1}{g_2}} \left(u_0(j, t) - \frac{1}{\sqrt{3}} \right), \quad (45)$$

where $u_0(j, t)$ is given by (41). The solution parameters m, a, b, c, d, ω and $\epsilon = \sqrt{(\hat{a}_c/\hat{a}) - 1}$ are established using the steps outlined in Section 4 (also refer to Figure 1). As previously explained, choosing \hat{a} and n/N then determines the remaining parameters.

The traffic model (1) governing headway is next solved with MATLAB's ode45, where the initial condition is defined by (45). As well, periodic boundary conditions are implemented. Then, over different time intervals, the asymptotic and numerical results are compared in Figures 2-5. Here, the number of cars on the road is set to 100.

For Figures 2-4, the top panel conveys the asymptotic solution (41) over the domain $j \in [0, 100]$ and $t \in [0, 100]$. The middle panel then compares the asymptotic solution in black to the red-dotted numerical result for $j = 0, 100, t \in [0, 100]$ (left) and $j \in [0, 100], t = 10, 000$ (right). Lastly, the bottom plot depicts the numerical solution for $j \in [0, 100]$ and $t \in [9600, 10000]$.

The first, downward solution for $v_{max} = 2, h_c = 4, \hat{a} = 1.99$ ($\epsilon = 0.0709$), $n = 1$ and $N = 100$ is shown in Figure 2, where $\kappa_1/\gamma = 0.037582$. The top panel reveals two distinct zones. These are, a cluster of vehicles with headway $h_{min} < h_c$ represented by the wave trough and a much smaller vehicle cluster with headway h_c corresponding to the wave peak. So, a vehicle travelling at the safety distance h_c decelerates due to a slower preceding vehicle and then endures a prolonged slow period with headway h_{min} . They then return to the safety distance momentarily to repeat this process. The middle panel of Figure 2 reveals excellent agreement between the two solutions. The numerical result at t very large is examined in the middle and lower panels, where the numerical wave appears to propagate without divergence, a change in amplitude or the development of a phase shift, when compared to the asymptotic solution. This suggests that this spatially periodic solution is stable.

Figure 3 portrays the alternate second solution for $v_{max} = 2, h_c = 4, \hat{a} = 1.99$ ($\epsilon = 0.0709$), $n = 1$ and $N = 100$, where $\kappa_1/\gamma = 0.219018$. The top panel shows it is of an upward form since now the headway varies between h_c and $h_{max} > h_c$. Therefore, a vehicle travelling at the safety distance h_c will now accelerate as the preceding car is faster. This vehicle then experiences an extended faster state, travelling with the headway h_{max} . Next, they decelerate and revert to the safety distance h_c . The car remains briefly at h_c and then repeats this motion. The middle panel shows again little discrepancy between the asymptotic and numerical solutions. As well, the middle right and bottom figures investigate the long time behaviour of the numerical result. Once again, no evidence of a phase shift or amplitude variation is exhibited and thus, this solution appears stable.

Next, the driver's sensitivity is reduced to $\hat{a} = 1.98$ and as a result, the perturbation parameter increases to $\epsilon = 0.1005$. The first solution is displayed in Figure 4 where $v_{max} = 2, h_c = 4, n = 1, N = 100$ and $\kappa_1/\gamma = 0.037578$. The vehicle behaviour is consistent with Figure 2, except now the wave trough is flatter and h_{min} has decreased. Hence, the duration of a car travelling with headway h_{min} is longer and the reduction in speed is greater. The middle panel depicts some very small differences between the asymptotic and numerical solutions due to increasing ϵ , although the match is still very good. Analysing the solution at t very large in the middle right and bottom figures, it is apparent that the numerical result is again stable since the phase and amplitude appear constant with increasing t . There is also a second, upward stable solution that corresponds to the parameters $\hat{a} = 1.98, v_{max} = 2, h_c = 4, n = 1$ and $N = 100$, although it is not depicted here. This solution will have the same behaviour as that conveyed by Figure 3, such that $\Delta x_j \in [h_c, h_{max}]$.

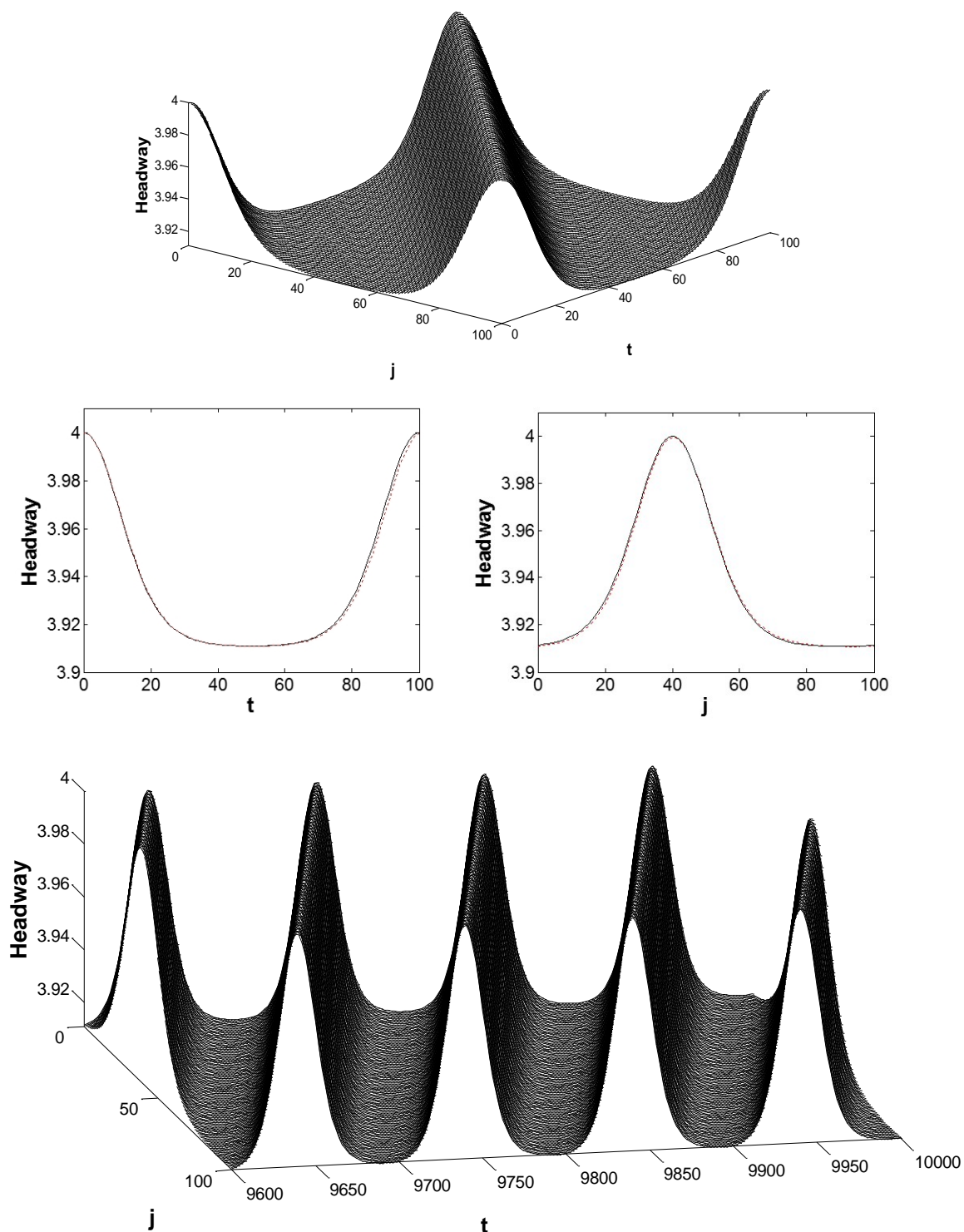


Figure 2: Headway solutions to the model (1) that satisfy periodic boundaries, where $m = 0.99659$, $\epsilon = 0.0709$, $\omega = 4.79$, $\hat{a} = 1.99$, $n = 1$, $N = 100$, $\kappa_1/\gamma = 0.037582$. Top: The asymptotic solution for $j \in [0, 100]$ and $t \in [0, 100]$. Middle left: The asymptotic solution (black) compared to the numerical solution (red dotted) when $j = 0, 100$ and $t \in [0, 100]$. Middle right: The asymptotic solution (black) compared to the numerical solution (red dotted) when $t = 10000$ and $j \in [0, 100]$. Bottom: The numerical solution for $j \in [0, 100]$ and $t \in [9600, 10000]$.

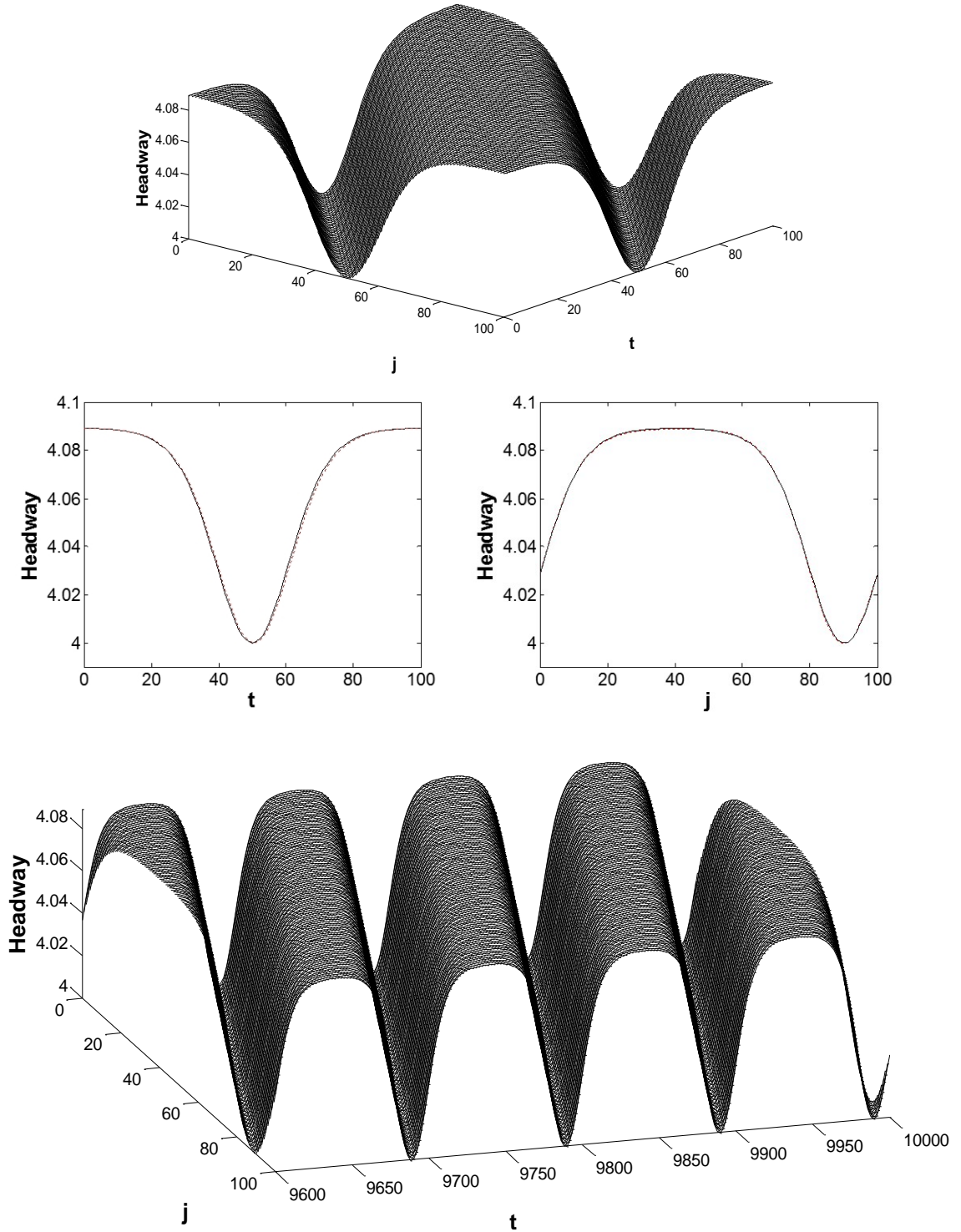


Figure 3: Headway solutions to the model (1) that satisfy periodic boundaries, where $m = 0.99659$, $\epsilon = 0.0709$, $\omega = 4.79$, $\hat{a} = 1.99$, $n = 1$, $N = 100$, $\kappa_1/\gamma = 0.219018$. Top: The asymptotic solution for $j \in [0, 100]$ and $t \in [0, 100]$. Middle left: The asymptotic solution (black) compared to the numerical solution (red dotted) when $j = 0, 100$ and $t \in [0, 100]$. Middle right: The asymptotic solution (black) compared to the numerical solution (red dotted) when $t = 10000$ and $j \in [0, 100]$. Bottom: The numerical solution for $j \in [0, 100]$ and $t \in [9600, 10000]$.

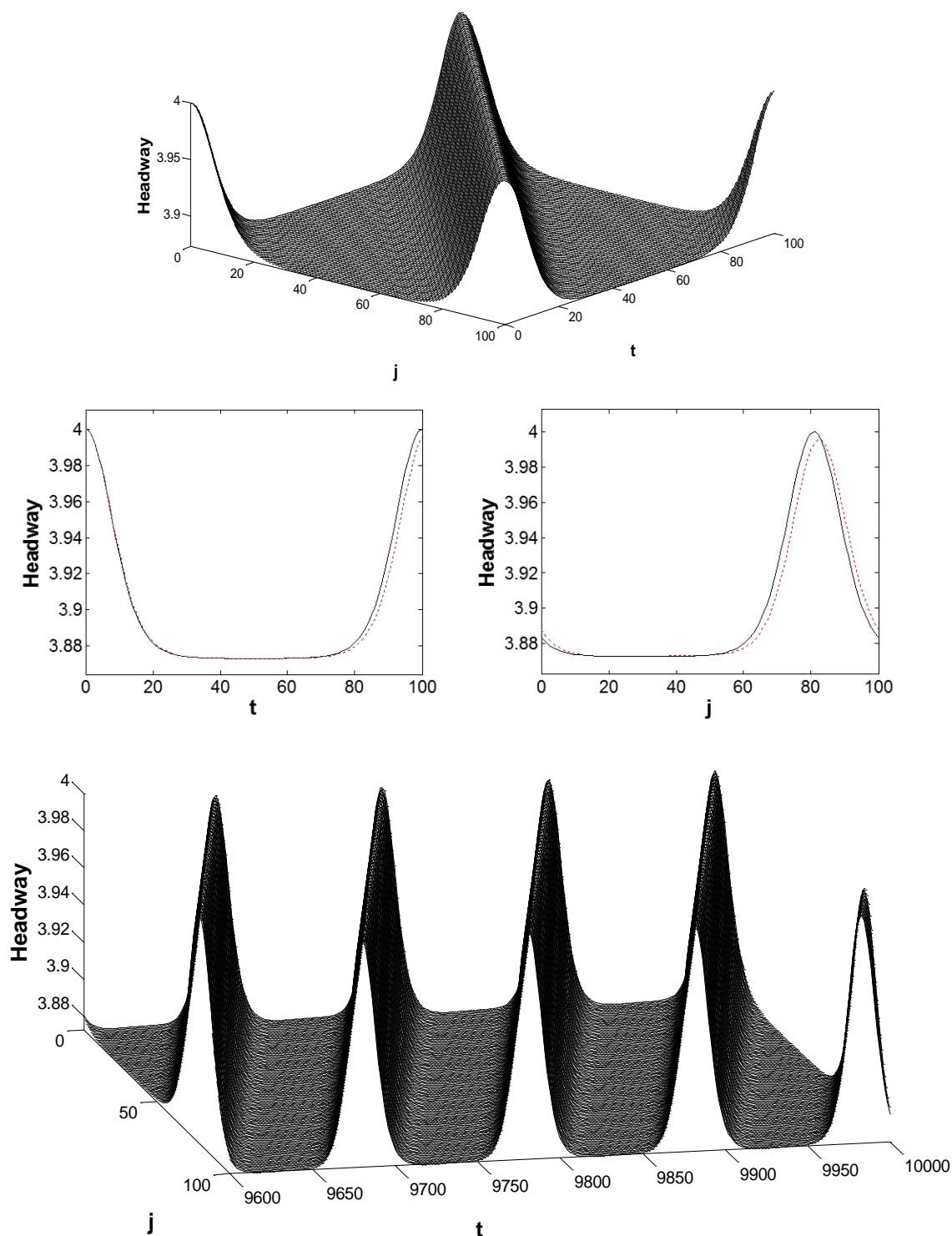


Figure 4: Headway solutions to the model (1) that satisfy periodic boundaries, where $m = 0.99987$, $\epsilon = 0.1005$, $\omega = 4.80$, $\hat{a} = 1.98$, $n = 1$, $N = 100$, $\kappa_1/\gamma = 0.037578$. Top: The asymptotic solution for $j \in [0, 100]$ and $t \in [0, 100]$. Middle left: The asymptotic solution (black) compared to the numerical solution (red dotted) when $j = 0, 100$ and $t \in [0, 100]$. Middle right: The asymptotic solution (black) compared to the numerical solution (red dotted) when $t = 10000$ and $j \in [0, 100]$. Bottom: The numerical solution for $j \in [0, 100]$ and $t \in [9600, 10000]$.

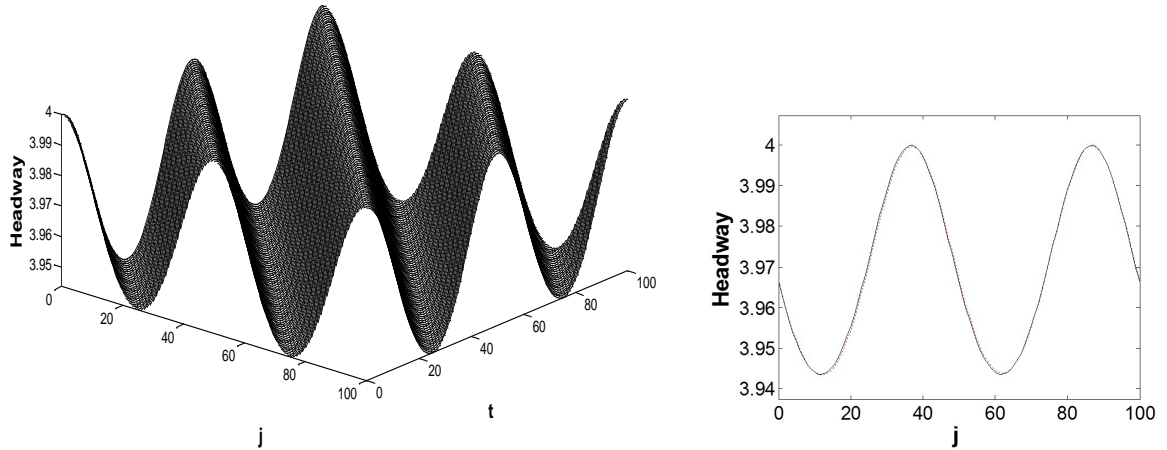


Figure 5: Headway solutions to the model (1) that satisfy periodic boundaries, where $m = 0.792877$, $\epsilon = 0.0709$, $\omega = 4.38$, $\hat{a} = 1.99$, $n = 2$, $N = 100$, $\kappa_1/\gamma = 0.051638$. Left: The asymptotic solution for $j \in [0, 100]$ and $t \in [0, 100]$. Right: The asymptotic solution (black) compared to the numerical solution (red dotted) when $t = 10000$ and $j \in [0, 100]$.

So far, the solutions considered all have one peak/trough over the domain $j \in [0, 100]$, since $n = 1$. Instead, choosing $n > 1$, multiple oscillations over the domain will occur. As an example, the downward solution corresponding to $\hat{a} = 1.99$, $v_{max} = 2$, $h_c = 4$, $n = 2$, $N = 100$, $\kappa_1/\gamma = 0.051638$ is shown in Figure 5. The behaviour observed on the left is consistent with $n = 1$ (Figure 2), except waves with two headway troughs/peaks over $j \in [0, 100]$ now propagate. The long time dynamics are examined on the right, where the black and red-dotted curves correspond to the asymptotic and numerical solutions respectively when $t = 10000$. The solution appears stable since no phase or amplitude changes are exhibited.

Thus, our set of periodic solutions have been shown to be stable using numerical results. In contrast, Komatsu and Sasa [1995] found solutions of a similar form that they supposed were always unstable, and therefore not observed numerically. Note however that our solutions are numerically stable only within a certain neighbourhood of the neutral stability line's critical point (see Section 2).

6 Conclusion

The OV model (1) was used to predict traffic behaviour. In particular, this model's linearly unstable region was studied, where (1) transformed into the mKdV equation with higher order correction terms. A multi-scale perturbation method was applied to this equation to locate steady travelling wave solutions. Consequently, the leading order solution that varied with slow and fast variables was defined. A system of differential equations at the next order was also found, which described this solution's slow evolution. The critical points of this system were shown to represent a family of steady travelling waves that had constant amplitude, mean height and period. Imposing periodic boundary constraints then determined the relationship between the solution parameters and the driver's sensitivity, \hat{a} , where for some fixed value of \hat{a} , two solutions existed of upward and downward form. As a result of establishing this relationship for \hat{a} , a numerical investigation was performed. This validated our analysis by demonstrating excellent agreement between the asymptotic and numerical results. Furthermore, we examined the behaviour of these solutions when t was very large. The numerical wave did not diverge, exhibit any phase shift or variation in amplitude, suggesting our set of solutions was stable. Identifying these stable solutions will

have important implications for future studies of the traffic model (1), particularly when numerically evaluating (1) within the unstable region and interpreting the results.

Appendix

The integrals α_1 and α_2 written in full are

$$\alpha_1 = \frac{1}{2P} \int_{\theta_1}^{\theta_2} u_0 d\theta = c + \frac{(d-c)}{2P} \int_{\theta_1}^{\theta_2} \frac{\text{sn}^2(\beta(\theta - \theta_0))}{e + \text{sn}^2(\beta(\theta - \theta_0))} d\theta,$$

$$\alpha_2 = \frac{1}{2P} \int_{\theta_1}^{\theta_2} u_0^2 d\theta = c^2 + \frac{2c(d-c)}{2P} \int_{\theta_1}^{\theta_2} \frac{\text{sn}^2(\beta(\theta - \theta_0))}{e + \text{sn}^2(\beta(\theta - \theta_0))} d\theta + \frac{(d-c)^2}{2P} \int_{\theta_1}^{\theta_2} \frac{\text{sn}^4(\beta(\theta - \theta_0))}{(e + \text{sn}^2(\beta(\theta - \theta_0)))^2} d\theta,$$

given (20). Using Byrd and Friedman [1954] to solve these integrals, we obtain

$$\begin{aligned} & \frac{1}{2P} \int_{\theta_1}^{\theta_2} \frac{\text{sn}^2(\beta(\theta - \theta_0))}{e + \text{sn}^2(\beta(\theta - \theta_0))} d\theta = 1 - \frac{\Pi(-1/e, m)}{K(m)}, \\ & \frac{1}{2P} \int_{\theta_1}^{\theta_2} \frac{\text{sn}^4(\beta(\theta - \theta_0))}{(e + \text{sn}^2(\beta(\theta - \theta_0)))^2} d\theta \\ & = \frac{1}{K(m)} (K(m) - 2\Pi(-1/e, m)) \\ & + \frac{1}{2K(m)(-1/e - 1)(m^2 + 1/e)} \left(-\frac{E(m)}{e} + (m^2 + 1/e)K(m) + \Pi(-1/e, m)(-2m^2/e - 2/e - 1/e^2 - 3m^2) \right), \end{aligned}$$

where K , E and Π are the complete elliptic integrals of the first, second and third kind respectively. Therefore, α_1 and α_2 are functions of the solution parameters m , c , d and e (see (20)).

References

- M. Bando, K. Hasebe, A. Nakayama, A. Shibata, and Y. Sugiyama. Dynamical model of traffic congestion and numerical simulation. *Phys. Rev. E*, 51:1035–1042, 1995.
- P. Byrd and M. Friedman. *Handbook of Elliptic Integrals for Engineers and Physicists*. Springer-Verlag, Berlin, 1954.
- H.X. Ge, R.J. Cheng, and S.Q. Dai. KdV and kink-antikink solitons in car-following models. *Physica A*, 357(34):466–476, 2005.
- L.L. Hattam. KdV cnoidal waves in a traffic flow model with periodic boundaries. *Physica D (under review)*, 2016.
- L.L. Hattam and S.R. Clarke. Modulation theory for the steady forced KdV-Burgers equation and the construction of periodic solutions. *Wave Motion*, 56(0):67–84, 2015.
- A.M. Kamchatnov, Y.-H. Kuo, T.-C. Lin, T.-L. Horng, S.-C. Gou, R. Clift, G.A. El, and R.H.J. Grimshaw. Undular bore theory for the Gardner equation. *Phys. Rev. E*, 86:036605–036627, 2012.
- T.S. Komatsu and S. Sasa. Kink soliton characterizing traffic congestion. *Phys. Rev. E*, 52:5574–5582, 1995.
- Z. Li, R. Zhang, S. Xu, and Y. Qian. Study on the effects of driver’s lane-changing aggressiveness on traffic stability from an extended two-lane lattice model. *Communications in Nonlinear Science and Numerical Simulation*, 24(1-3):52–63, 2015.

- M. Muramatsu and T. Nagatani. Soliton and kink jams in traffic flow with open boundaries. *Phys. Rev. E*, 60:180–187, 1999.
- T. Nagatani. The physics of traffic jams. *Rep. Prog. Phys.*, 65(9):1331, 2002.
- L.-J. Zheng, C. Tian, D.-H. Sun, and W.-N. Liu. A new car-following model with consideration of anticipation driving behavior. *Nonlinear Dynamics*, 70(2):1205–1211, 2012.
- H.B. Zhu and S.Q. Dai. Numerical simulation of soliton and kink density waves in traffic flow with periodic boundaries. *Physica A*, 387(16-17):4367–4375, 2008.